Proceeding of the IEEE
International Conference on Robotics and Biomimetics
Dali, China, December 2019

2-DOF Simultaneous Control of Dexterous Prosthesis based on Constrained NMF and Hadamard Product*

Zixin Wang[1,2], Dapeng Yang[1,3], Jiaming Li[1], Hong Liu[1]

1.State Key Laboratory of Robotics and System, 2.School of Foreign Language, 3.Artificial Intelligence Laboratory
Harbin Institute of Technology,
Harbin 150081, China

{wangzx97, yangdapeng, 17s008059, hong.liu}@hit.edu.cn

***Abstract* - It is a question of great import for the dexterous prosthesis to realize its continuous, simultaneous and proportional control of multi-DOFs so that its rehabilitation function can be well achieved and its user acceptance rate can be improved. In this paper, we propose a new method, CNMF-HP, which integrates the constrained non-negative matrix factorization (NMF) and the Hadamard product, for estimating 2-DOF wrist movements (DOF-1, flexion/extension; DOF-2, adduction/abduction) from myoelectric signals. Based on this method, the simultaneous control of a multi-fingered prosthesis is verified in this paper. Through establishing the mapping relationship between the wrist movements and the finger movements of the dexterous prosthesis, two grasp control strategies (synchronous and asynchronous) are proposed and successfully applied in operating the dexterous prosthesis to grasp four kinds of objects of different grasping patterns (cylindrical, spherical, tripod and lateral). Then, the performance of different strategies (synchronous/asynchronous control) in the grasping process is compared in terms of the completion time and completion rate of the tasks, in this way the superiority of EMG control proposed in this paper is further verified.**

Index Terms* - *myoelectric signal, NMF, simultaneous and proportional control, motion decoding.

I. Introduction

The rehabilitation function of a hand prosthesis relies on the dexterity of the mechanical body and the intuitive control methods matched with it. At present, the multi-DOF dexterous prosthesis is becoming more and more popular, and there are two main methods are adopted in its control. One is to discriminate the myoelectric (electromyogram, EMG) pattern by using pattern recognition [1-3], while only one movement can be controlled at a time (discrete control) so that its flexibility and continuity of operation is relatively poor. The other is based on the regression method [4, 5], which estimates the continuous motion parameters of multiple joints from EMG signals so as to realize a multi-DOF simultaneous control.

On the premise of satisfying the hypothesis of a linear system, the non-negative matrix factorization (NMF) is widely used as a decoding algorithm to estimate the joint motion parameters continuously. Jiang et al. established a synergy matrix model of the activating muscles and used NMF[6] to extract the force vector of each joint from the sEMG feature (mean square value, MSV) [7, 8]. Based on this, Ma et al. investigated the influence of different EMG features on the decoding accuracy [9] and found that the features as mean absolute value (MAV), RMS, and waveform length (WL) were superior in the NMF algorithm. Further results on this topic have shown that the NMF was robust to the number of channels and the placement of electrodes [10], but the decoupling accuracy among DOFs was not ideal. To solve this issue, Lin et al. introduced the $L1$ norm regular term in the model (SCNMF) [11], so as to improve the sparsity when decomposing the matrix to a certain extent. However, when a single DOF is just needed to be activated in some simple tasks, the decoding signal of the other DOF(s) cannot be effectively suppressed. As well, the performance of the method could vary greatly when giving different matrix initialization conditions. Kim et al. proposed to use Hadamard product (NMF-HP) [12] to specify the elements in the activation coefficient vector (ACV) with related to inactivated DOFs as zeros, so as to ensure that the respective ACVs of different DOFs obtained by NMF could be fully decoupled. However, model over-fitting might be aroused, since the method reused the calibration matrix of EMG feature in the following prediction.

On refining these existing methods, this paper proposes a new method, CNMF-HP, based on which the on-line control of the dexterous prosthesis (HITAPH 5) is realized, and the effectiveness of this method is verified.

II. Methods

A. Algorithms

1) NMF, SCNMF, and NMF-HP

The result obtained by NMF has a clear physical meaning since there is no negative element [13, 14]. Therefore, it is suitable to be used in extracting the neural driving strength of the joints from sEMG signals. If the noise between EMG channels can be neglected and suitable features are selected, the muscle synergy matrix [6] can be adopted as a theoretical model for achieving a superior motor decoding. The time-domain (TD) features of sEMG, like root mean square (RMS), are approximately linear with the joint forces, which can be expressed as

* This work is partially supported by the National Key R&D Program of China Grant #2018YFB1307201 to L. Jiang, and the NSF Grant #51675123 and Postdoctoral Scientific Research Development Fun (LBH-W18058) to D.Yang . Corresponding author: Dapeng Yang (yangdapeng@hit.edu.cn).

978-1-7281-6321-5/19//$31.00 ©2019 IEEE

$$\boldsymbol{Z}(t) \approx W \cdot \boldsymbol{F}(t) = [\boldsymbol{W}_1^+ \ \boldsymbol{W}_1^- \cdots \boldsymbol{W}_N^+ \ \boldsymbol{W}_N^-] \cdot \begin{bmatrix} \boldsymbol{F}_1^+(t) \\ \boldsymbol{F}_1^-(t) \\ \cdots \\ \boldsymbol{F}_N^+(t) \\ \boldsymbol{F}_N^-(t) \end{bmatrix}, \quad (1\text{-a})$$

where $\boldsymbol{Z}(t)_{M\times 1}$ is the TD feature vector extracted from the M channels of sEMG at time t; $\boldsymbol{W}_{M\times 2N}$ is the muscle synergy matrix; $\boldsymbol{F}(t)_{2N\times 1}$ is the activation coefficients on each DOF; the upper corner '+' and '−' represents the positive and negative direction, respectively. When considering the time sequence of sEMG, we can re-write (1-a) as:

$$\boldsymbol{Z}_{M\times L} \approx \boldsymbol{W}_{\mathrm{M}\times 2\mathrm{N}} \cdot \boldsymbol{F}_{2N\times \mathrm{L}}, \quad (1\text{-b})$$

where M is the number of channels; L is the number of sEMG samples; N is the number of DOFs. And the elements of each matrix in (1-b) should be all non-negative.

To resolve $\boldsymbol{F}$ from $\boldsymbol{Z}$ in real-time, we should get some prior knowledge about $\boldsymbol{W}$ through a calibration procedure. In this procedure, the EMG samples $\boldsymbol{Z}$ with labels $\boldsymbol{F}$ are collected and used to find a suitable $\boldsymbol{W}$ through NMF. In the traditional method like [6], the EMG samples are collected only with single-DOF movements. Then, the NMF is utilized to extract the DOF-related synergy vectors, which are further rearranged together to obtain the synergy matrix $\boldsymbol{W}$. Since no EMG samples of multi-DOF movements are collected, the decoupling accuracy among DOFs is relatively low, so that the accuracy of single-DOF movement can not be guaranteed. In order to make a distinction among synergy vectors corresponding with different DOFs as much as possible and to better decouple the DOFs of each joint, sparse constraints, such as $L1$ norm regular term [11] and Hadamard product [12], are often added to the matrix.

The $L1$ norm, which represents the sum of the absolute values of all elements, is an important index affecting the sparse degree of the matrix. Lin et al. added $L1$ norm regular term to the activation coefficient matrix column vector [11] (termed as SCNMF, hereafter) in traditional NMF algorithm,

$$\min_{\boldsymbol{W},\boldsymbol{F}} \frac{1}{2}\|\boldsymbol{Z} - \boldsymbol{W}\cdot\boldsymbol{F}\|_{Fro}^2 + \lambda \sum_{l=1}^{L} \|\boldsymbol{F}(:,l)\|_1^2 \ s.t. \boldsymbol{W},\boldsymbol{F} \geq 0, \quad (2)$$

where $\boldsymbol{F}(:,l)$ is the first column vector of the activation matrix; 'Fro' is the Frobenius norm; λ is the regular term coefficient, which is used to balance the accuracy and sparsity of the matrix. The objective function can be re-written in matrix form,

$$\min_{\boldsymbol{W},\boldsymbol{F}} \left\| \begin{pmatrix} \boldsymbol{W} \\ \sqrt{\lambda} e_{1\times 2N} \end{pmatrix} \boldsymbol{F} - \begin{pmatrix} \boldsymbol{Z} \\ 0_{1\times N} \end{pmatrix} \right\|_{Fro}^2 s.t. \boldsymbol{W},\boldsymbol{F} \geq 0, \quad (3)$$

where $e_{1\times 2N}$ and $0_{1\times L}$ are row vectors with all elements as 1 and 0 respectively.

Though the SCNMF algorithm adds sparsity to the overall matrix, it cannot specify the sparsity of specific elements in the matrix. Kim et al. proposed to apply the constraint matrix $\boldsymbol{C}$ to the activation coefficient matrix $\boldsymbol{F}$ by using the Hadamard product (termed as NMF-HP, hereafter) [12]. At this time, the muscle synergy matrix can be re-written as

$$\boldsymbol{Z}(t) \approx \boldsymbol{W} \cdot (\boldsymbol{C} \circ \boldsymbol{F}), \quad (4)$$

where $\boldsymbol{C}$ is the constraint matrix, whose elements reflect the activation condition (0 or 1) of the synergies corresponding to each DOF. The circle in (4) represents the Hadamard product, of which the matrix dimension on both sides are the same, and the corresponding elements are multiplied. Through this approach, it can be ensured that the calibrated activation coefficient vectors among each DOF can be fully decoupled.

2) The proposed Method: CNMF-HP

Due to the strong sparse effect of the constrained matrix, it is easy for NMF-HP algorithm to be over-fitting in calibration, in which way the estimation accuracy of joint motion parameters will be affected. We emphasis on improving the generalization capability of synergy matrix $\boldsymbol{W}$ to avoid the overdependence of the algorithm on the EMG data adopted in calibration. Considering that $L2$ norm is an important index affecting the structural complexity of the algorithm, in order to simplify the model and enhance the robustness of the algorithm and the reliability of EMG control method, the NMF-HP algorithm is further improved in this paper. In specific, the $L2$ norm regular term of the synergy vector is added to the objective function, that is:

$$\min_{\boldsymbol{W},\boldsymbol{F}} \frac{1}{2}\|\boldsymbol{Z} - \boldsymbol{W}\cdot(\boldsymbol{C}\circ\boldsymbol{F})\|_{Fro}^2 + \lambda \sum_{m=1}^{M} \|\boldsymbol{W}(m,:)\|_2^2 \ s.t. \boldsymbol{W},\boldsymbol{F} \geq 0, \quad (5)$$

where, $\boldsymbol{W}(\mathrm{m},:)$ is the m-th row vector of the synergy matrix; λ is the regular term coefficient, which is used to balance the influence of the calibration feature data set on the model. The value of λ can be selected by off-line cross-validation analysis, and (5) can be rewritten into its matrix form

$$\min_{\boldsymbol{W},\boldsymbol{F}} \|\boldsymbol{W}\cdot[\boldsymbol{C}\circ\boldsymbol{F}, \sqrt{\lambda}\boldsymbol{I}_{2N\times 2N}] - [\boldsymbol{Z}, \boldsymbol{0}_{M\times 2N}]\|_{Fro}^2 \ s.t. \boldsymbol{W},\boldsymbol{F} \geq 0, \quad (6)$$

where $\boldsymbol{0}_{M\times 2N}$ is a null matrix, and $\boldsymbol{I}_{2N\times 2N}$ is an identity matrix.

B. Model Calibration

1) Data Collection protocol

The Myo armband (Thalmic Labs Inc., USA) was used to collect the raw sEMG signals. The eight electrodes were placed around the apex of the subject's forearm muscle bulge equidistantly. A real-time wireless transmission (Bluetooth) of the EMG signals into the laptop (LabVIEW) was realized through UDP protocol. In addition, the RMS feature extracted from a 100ms window (sampling frequency of 200Hz, 20 points) was used as the input of the model.

Sitting by a table, the subject needed to prop the elbows up on the table, at the same time keep the hand open and perpendicular to the table. Through the data collection software (Fig.1-a), the subject needed to collect the EMG signals of four groups of motions (Fig.1-b) in turn according to the guidance of the instructive cursor, which was used for the calibration of the model. Each motion lasts about 20s (200 samples), during which the cursor moved reciprocally around the origin at different rates. Besides, when the indicating cursor was at its limit position, the subject was required to keep the muscle around the maximal voluntary contraction (MVC).

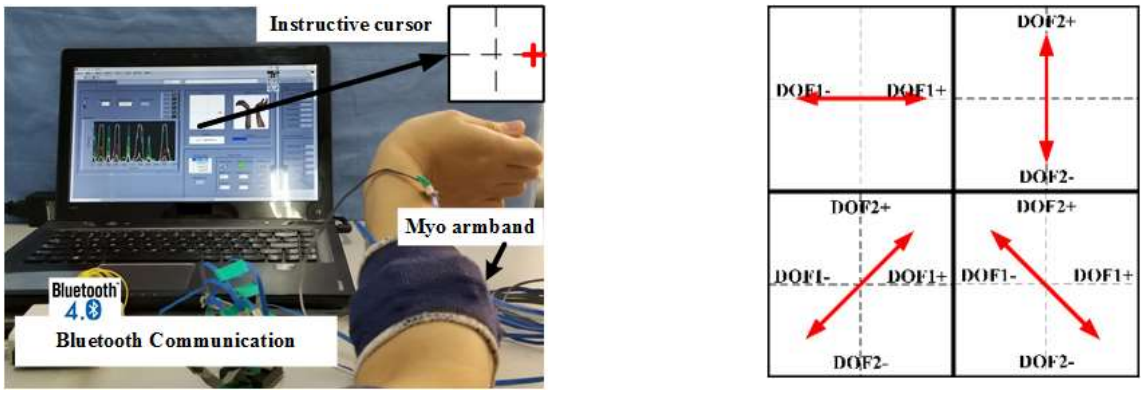

a) b)

Fig.1 The data collection platform (a) and four motions (b) needed to be collected. In (b), the DOF1 denotes the wrist flexion/extension, while the DOF2 denotes the wrist adduction/abduction (radial/ulnar deviation).

2) Model Calibration

This paper focuses on the 2-DOF movements of the wrist (DOF-1, the extension/flexion of the wrist, DOF-2, the adduction/abduction of the wrist, N=2). The EMG signals, collected from two single-DOF motions and two 2-DOF simultaneous motions (Fig.1-2), were contained in one dataset used for model calibration. Assuming that the number of samples collected under each motion is L, according to (4), the muscle synergy matrix model with Hadamard product can be expressed as

$$\boldsymbol{Z} \approx \boldsymbol{W} \cdot \left(\begin{bmatrix} \mathbf{1}_{1\times L} & \mathbf{0}_{1\times L} & \mathbf{1}_{1\times L} & \mathbf{1}_{1\times L} \\ \mathbf{1}_{1\times L} & \mathbf{0}_{1\times L} & \mathbf{1}_{1\times L} & \mathbf{1}_{1\times L} \\ \mathbf{0}_{1\times L} & \mathbf{1}_{1\times L} & \mathbf{1}_{1\times L} & \mathbf{1}_{1\times L} \\ \mathbf{0}_{1\times L} & \mathbf{1}_{1\times L} & \mathbf{1}_{1\times L} & \mathbf{1}_{1\times L} \end{bmatrix} \circ \begin{bmatrix} \boldsymbol{F}_{11}^{+} & \boldsymbol{F}_{12}^{+} & \boldsymbol{F}_{13}^{+} & \boldsymbol{F}_{14}^{+} \\ \boldsymbol{F}_{11}^{-} & \boldsymbol{F}_{12}^{-} & \boldsymbol{F}_{13}^{-} & \boldsymbol{F}_{14}^{-} \\ \boldsymbol{F}_{21}^{+} & \boldsymbol{F}_{22}^{+} & \boldsymbol{F}_{23}^{+} & \boldsymbol{F}_{24}^{+} \\ \boldsymbol{F}_{21}^{-} & \boldsymbol{F}_{22}^{-} & \boldsymbol{F}_{23}^{-} & \boldsymbol{F}_{24}^{-} \end{bmatrix} \right), \quad (7)$$

where $\mathbf{1}_{1\times L}$ and $\mathbf{0}_{1\times L}$ are row vectors with all elements as 1 and 0 respectively, which reflects the activation of corresponding DOFs; $\boldsymbol{F}_{ij}^{+(-)}$ is the activation coefficient vector of the positive (negative) direction of the i-th DOF and the j-th motion.

With the introduction of the Hadamard product, the W in (7) was solved by alternating non-negative least-squares [15]

$$\boldsymbol{W}^{(k+1)} = \underset{\boldsymbol{W}>0}{\operatorname{argmin}} \left\| \boldsymbol{W} \cdot \left[\boldsymbol{C}\circ\boldsymbol{F}, \sqrt{\lambda}\boldsymbol{I}\right]^{(k)} - [\boldsymbol{Z}, 0] \right\|_{Fro}^{2}, \quad (8\text{-a})$$

$$\left[\boldsymbol{C}\circ\boldsymbol{F}, \sqrt{\lambda}\boldsymbol{I}\right]^{(k+1)} = \underset{\boldsymbol{F}>0}{\operatorname{argmin}} \left\| \boldsymbol{W}^{(k+1)} \cdot \left[\boldsymbol{C}\circ\boldsymbol{F}, \sqrt{\lambda}\boldsymbol{I}\right] - [\boldsymbol{Z}, 0] \right\|_{Fro}^{2}, \quad (8\text{-b})$$

where multiplicative iterative was adopted so that the zero terms can remain unchanged in the iterative procedure. Processing $\left[\boldsymbol{C}\circ\boldsymbol{F}, \sqrt{\lambda}\boldsymbol{I}\right]$ as a whole, then from which the activation coefficient matrix $\boldsymbol{F}$ was obtained through extracting the first L column directly after the iteration finished.

When estimating $\boldsymbol{F}$ in real-time, the matrix $\widetilde{\boldsymbol{W}} = (\boldsymbol{C}\circ\boldsymbol{F}) \cdot \boldsymbol{Z}^{+}$, instead of the pseudo-inverse matrix $\boldsymbol{W}^{+}$, was used to ensure the estimation accuracy. The activation coefficient matrix $\widetilde{\boldsymbol{F}}(t)$ was estimated through left-multiplying $\widetilde{\boldsymbol{W}}$ by the sEMG feature matrix $\widetilde{\boldsymbol{Z}}(t)$, as shown in (9)

$$\widetilde{\boldsymbol{F}}(t) = \widetilde{\boldsymbol{W}} \cdot \widetilde{\boldsymbol{Z}}(t) = \begin{bmatrix} \widetilde{\boldsymbol{F}}_1^{+}(t) \\ \widetilde{\boldsymbol{F}}_1^{-}(t) \\ \widetilde{\boldsymbol{F}}_2^{+}(t) \\ \widetilde{\boldsymbol{F}}_2^{-}(t) \end{bmatrix} \quad (9)$$

By linearly combining the activation coefficient vector corresponding to the two synergies under the same DOF, the control signal for this DOF can be obtained. The relationship between the control signal and the activation coefficient vector is shown as

$$\begin{cases} \widetilde{\boldsymbol{F}}_1(t) = \tau_{11}\widetilde{\boldsymbol{F}}_1^{+}(t) - \tau_{12}\widetilde{\boldsymbol{F}}_1^{-}(t) \\ \widetilde{\boldsymbol{F}}_2(t) = \tau_{21}\widetilde{\boldsymbol{F}}_1^{+}(t) - \tau_{22}\widetilde{\boldsymbol{F}}_1^{-}(t) \end{cases}, \quad (10)$$

where the weight of the activation coefficient $\boldsymbol{\tau}_{ij}$ needed to be adjusted in accordance with the sEMG strength, and it can be automatically calibrated during the online experiment. The MVC was pre-tested to configure the weight of activation coefficient$\boldsymbol{\tau}_{ij}$. The properly adjusted $\boldsymbol{\tau}_{ij}$ can ensure that when the cursor was controlled by the subjects, the voluntary contraction of the muscle was within 30% MVC.

More details on the comparison of using the new method (CNMF-HP) to the others (NMF, SCNMF, NMF-HP, etc) can be found in [16].

C. Online control

1) Test Platform

The experimental platform of the prosthesis control was built to verify the effectiveness of the proposed method. The EMG data received through Bluetooth was sent to the UDP port of the desktop computer. A software was developed in LabVIEW to realize EMG data acquisition/storage and model calibration. After calibration, the EMG signals can be predicted in real-time and the 2-channel control signals were output. Besides, the mapping relationship between the human wrist's DOFs and the prosthetic hand's DOFs was established. Then, the motion speeds of the six joints of the prosthetic hand were configured (the 100% MVC corresponds to the maximum speed), and the motion command was sent to the prosthesis HITAPH 5) in real-time through the LabVIEW VISA serial port, as shown in Fig.2.

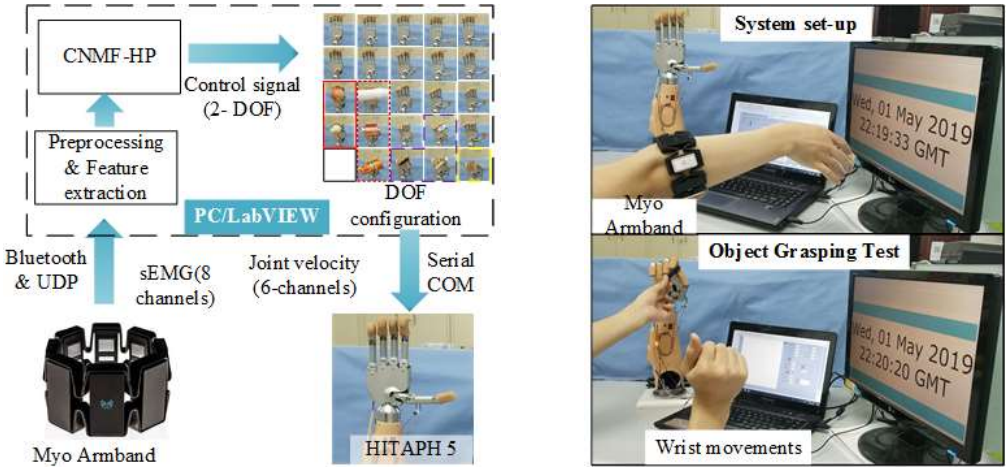

a) Data streaming b) Experiment procedure

Fig.2 The online hand grasp platform.

2) Control Strategy

The wrist flexion/extension and wrist radial/ulnar deviation were mapped into the thumb adduction/abduction and the hand opening/closing respectively. In detail, the wrist flexion and ulnar deviation were taken as the negative directions of DOF-1 and DOF-2, which were used to control the adduction of the thumb and the closing of the five fingers; while the wrist extension and radial deviation were taken as the positive directions of DOF-1 and DOF-2, being used to control the abduction of the thumb and the opening of the five fingers, as shown in Fig.3. Four typical grasping patterns (cylindrical, spherical, tripod, and lateral) that can be realized through controlling these two DOFs at the same time were also given in the figure.

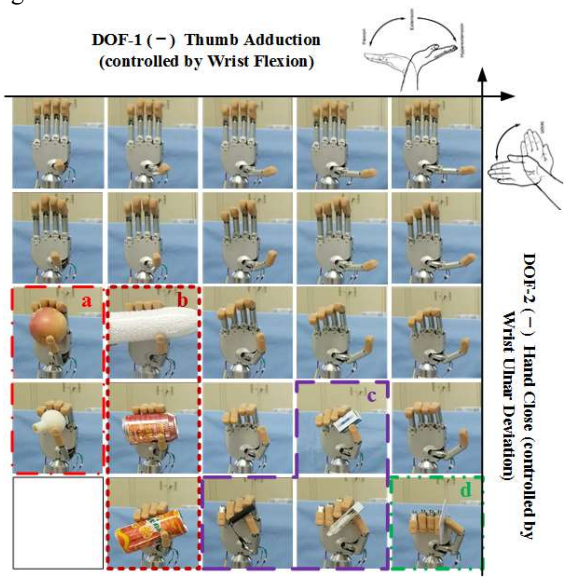

Fig. 3 2-DOF simultaneous control on finger motion: a) spherical grasp; b) cylindrical grasp; c) tripod grasp and d) lateral grasp.

In such kind of simultaneous control strategy (SCS), the 2-channel control signals output by the decoding mode CNMF-HP would be regarded as gains multiplied to the speed value of each joint of the hand (configured beforehand). These speed signals were sent to the hand prosthesis as motion commands. Therefore, by synchronously adjusting the movement direction and the muscle contraction force of the wrist joint, the subject can adjust the speed ratio of the 2-DOF control signals and then drive each joint of the prosthesis move simultaneously to grasp the objects.

To compare with the strategy above, an asynchronous control strategy (ACS) was also proposed. The ACS compared the size of the 2-channel control force signals and selected the DOF with larger absolute value as the activating DOF (the DOF with smaller absolute value will be suppressed). In the ACS, subjects can only use the dominant wrist motion (single-DOF, one by one) to drive the prosthesis joints to move to the final position of a given grasp pattern.

3) Task and Metrics

In this paper, 20 kinds of commonly-used objects were selected in accordance with four kinds of grasping mode (spherical grasp, cylindrical grasp, tripod grasp, and lateral grasp, evenly distributed). The grasping time and completion rate (whether the items can be grasped stably) of the grasps were taken as main indicators to evaluate the performance of different control methods.

During the experiment, the subject needed to wear electrodes on their right arms, used the left hand to grasp the 20 objects randomly and handed it over to the prosthesis. When the object came into the range of sight, the subject operated his right wrist and then drove the prosthesis to grasp the object according to its grasp pattern. In a set of experiment, all 20 objects needed to be grasped once and each time only one object was grasped. The same grasping strategy, SCS or ACS, was adopted in each set. A total of 10 sets of experiments needed to be done per day, in which the SCS and ACS were carried out alternately. The experiment lasted for four days, and a total of 40 groups of experiment and 800 grasps (20 items/set×5 sets/grasping patterns×2 grasping strategies×4 days) were obtained for each subject.

When evaluating the results, a grasp can be considered to be a success if the object can be firmly grasped by the prosthetic hand in a correct pattern; otherwise, a selection of a wrong grasp pattern, or unexpected drop of the object, would be all considered to be a failure. For each grasp, the timing began with the movement of the subject's right wrist and stopped with the completion or failure of the grasp. Afterward, the prosthesis was controlled to be back to its neutral position, and this period was not included in the grasp time of the object.

To evaluate the effectiveness of different grasping strategies (SCS and ACS), the grasping time t_g and the completion rate of the task r were adopted as evaluation indexes to statistically analyze the results on the four different grasp patterns. In addition, in order to avoid abnormal values, the failed data points were eliminated when the index t_g was counted.

III. Results & Discussions

The control signals output by CNMF-HP is combined with the hand postures to further analyze the grasping process, as shown in Fig.4. It shows that combining SCS with CNMF-HP, direct control of the two DOFs of the prosthesis (hand close and thumb abduction) can be ensured, and the operation is relatively simple and fluent. Also, a clear simultaneous and proportional control effect can be seen as the prosthesis is flexibly operated to complete the grasp tasks. Compared with the ACS, the operation complexity is reduced and the grasping time is significantly saved (p<0.05, except for lateral grasp, because it only refers to hand open/close).

The statistics of grasping time and the completion rate of the tasks under different control strategies are shown in Table 1 and Table 2. The results show that the SCS outperforms ACS in accomplishing the 2-DOF grasping task. The index t_g shortened by about 36% in three kinds of grasp patterns having two DOFs (except for lateral grasp that only one DOF, the thumb, is needed). Besides, with the increase of grasping times and testing days, the grasp performance under SCS improves more stably, which indicates that better control effect can be achieved through short-time learning. What's more, compared with [18], the SCS proposed in this paper does not need to obtain the grasping dataset of the prosthetic hand to extract synergies. Also, it seemed to outperform traditional methods in the completion rate and the grasping time.

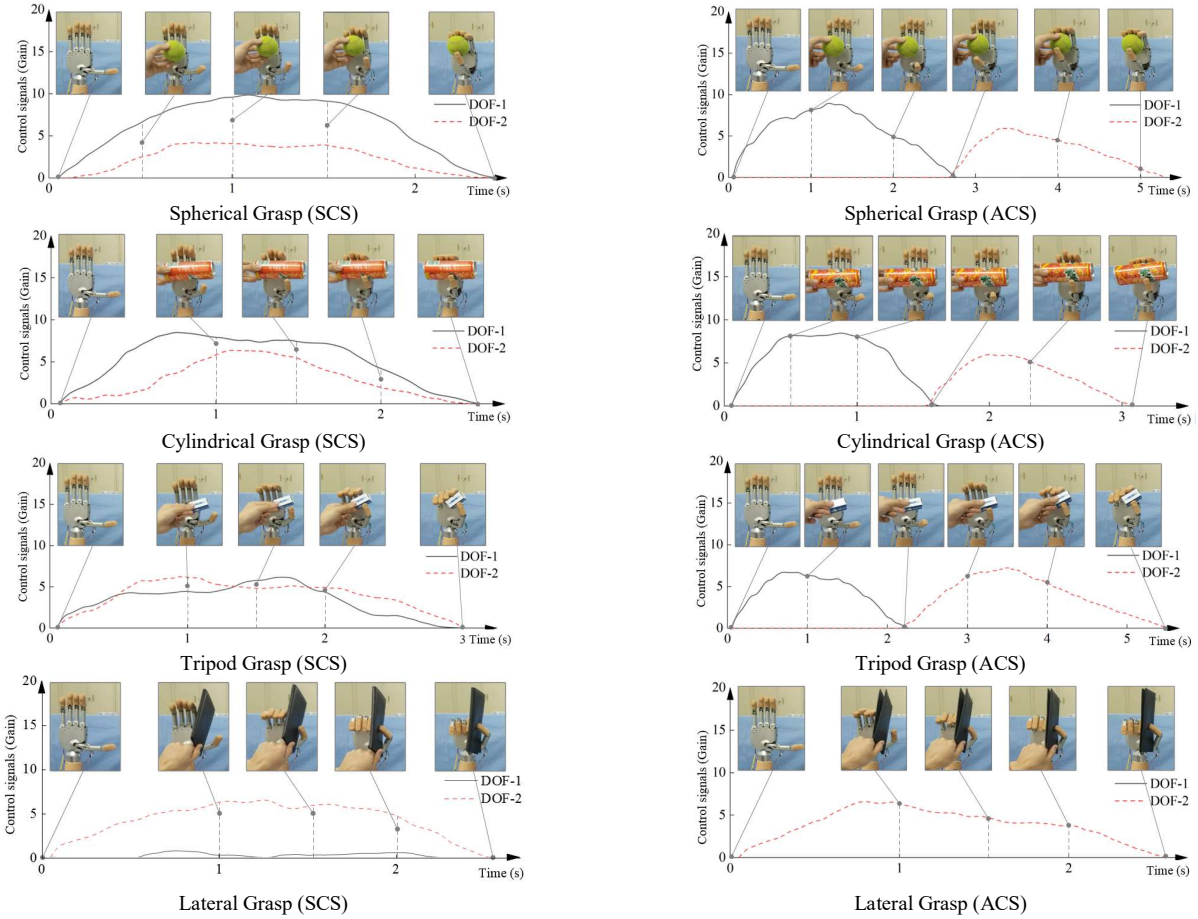

Fig.4 Comparison of the two-DOF simultaneous (left) and asynchronous control (right) on four grasp patterns.

TABLE I
STATISTICS ON THE MISSION COMPLETION TIME t_g USING DIFFERENT CONTROL STRATEGIES (S)

	Spherical		Cylindrical		Tripod		Lateral	
	SCS	ACS	SCS	ACS	SCS	ACS	SCS	ACS
Day 1	4.1±1.0	6.1±0.6	4.6±0.8	5.8±1.1	4.0±0.8	6.5±1.2	4.9±1.1	5.0±1.0
Day 2	4.0±0.7	5.9±0.8	3.8±0.9	5.1±0.8	3.9±0.6	6.0±0.7	4.6±0.7	4.8±0.9
Day 3	2.9±0.6	4.6±0.8	2.7±0.7	4.1±0.8	3.0±0.6	4.8±0.8	3.0±0.6	3.5±0.6
Day 4	2.5±0.6	4.2±0.9	2.5±0.6	3.6±0.5	2.5±0.5	3.9±0.8	2.7±0.5	2.8±0.6

TABLE II
STATISTICS ON THE MISSION COMPLETION RATE r USING DIFFERENT CONTROL STRATEGIES (%)

	Spherical		Cylindrical		Tripod		Lateral	
	SCS	ACS	SCS	ACS	SCS	ACS	SCS	ACS
Day 1	96	92	76	92	92	76	92	88
Day 2	100	92	96	92	100	88	96	100
Day 3	100	100	96	100	88	88	100	100
Day 4	100	100	100	100	100	92	100	100

In summary, through mapping the 2-DOF wrist movements to the finger movements of the hand prosthesis, the two DOFs of the hand can be successfully controlled in a simultaneous and proportional manner. The strategy SCS reduces the operational complexity with comparison to the ACS. In the experiment, the SCS takes shorter time in grasping and it is with higher grasping flexibility, which verifies the effectiveness of the simultaneous control method (CNMF-HP) proposed in this paper. In comparison, the ACS adopts single-DOF wrist movements sequentially to manipulate the corresponding individual DOF of the hand prosthesis, which is similar to the traditional method using hardware/software switch to activate the necessary DOF (switching control). The grasping time is longer because the two DOFs cannot be controlled synchronously; however, since the control amplitude of the two DOFs can be adjusted, it also has superior grasping flexibility when compared with the switching method. In addition, the grasping process using SCS is with higher continuity, which indicates that the CNMF-HP control method has a better performance in decoupling the two-DOF wrist movements.

IV. CONCLUSIONS

In this paper, based on refining the existing methods on simultaneous control, the constraint matrix and the Hadamard product were adopted to propose a new motion decoding method, CNMF-HP, and its on-line performance on operating a multi-DOF dexterous hand prosthesis was evaluated. Compared with traditional methods, the effectiveness of this method was examined. In further study, the experiment on more subjects will be carried out to explore the feasibility of this method in the control of the prosthesis.

REFERENCES

[1] T. A. Kuiken, L. A. Miller, K. Turner, and L. J. Hargrove, "A Comparison of Pattern Recognition Control and Direct Control of a Multiple Degree-of-Freedom Transradial Prosthesis," *IEEE Journal of Translational Engineering in Health and Medicine,* vol. 4, pp. 1-8, 2016.

[2] S. Zhang, X. Zhang, S. Cao, X. Gao, X. Chen, and P. Zhou, "Myoelectric Pattern Recognition Based on Muscle Synergies for Simultaneous Control of Dexterous Finger Movements," *IEEE Trans. Neural Syst. Rehabil. Eng.,* vol. 47, pp. 576-582, 2017.

[3] J. L. Betthauser, C. L. Hunt, L. E. Osborn, M. R. Masters, G. Lévay, R. R. Kaliki*, et al.*, "Limb Position Tolerant Pattern Recognition for Myoelectric Prosthesis Control with Adaptive Sparse Representations From Extreme Learning," *IEEE Trans. Neural Syst. Rehabil. Eng.,* vol. 65, pp. 770-778, 2018.

[4] I. Vujaklija, V. Shalchyan, E. N. Kamavuako, N. Jiang, H. R. Marateb, and D. Farina, "Online mapping of EMG signals into kinematics by autoencoding," *J Neuroeng Rehabil,* vol. 15, pp. 21-29, 2018/03/13 2018.

[5] J. M. Hahne, M. A. Schweisfurth, M. Koppe, and D. Farina, "Simultaneous control of multiple functions of bionic hand prostheses Performance and robustness in end users," *SCIENCE ROBOTICS,* vol. 3, p. eaat3630, 2018.

[6] N. Jiang, P. A. Parker, and K. B. Englehart, "Spectrum of the nonstationary electromyographic signal modeled with integral pulse frequency modulation and its application to estimating neural drive information," *J ELECTROMYOGR KINES,* vol. 19, pp. e267-e279, 2009/08/01/ 2009.

[7] N. Jiang, K. B. Englehart, and P. A. Parker, "Extracting simultaneous and proportional neural control information for multiple-dof prostheses from the surface electromyographic signal," *IEEE Transactions on Biomedical Engineering,* vol. 56, pp. 1070-1080, 2009.

[8] H. Rehbaum, N. Jiang, L. Paredes, S. Amsuess, B. Graimann, and D. Farina, "Real-time simultaneous and proportional control of multiple degrees of freedom from surface EMG: preliminary results on subjects with limb deficiency," in *Engineering in Medicine and Biology Society (EMBC), 2012 Annual International Conference of the IEEE*, 2012, pp. 1346-1349.

[9] J. Ma, N. V. Thakor, and F. Matsuno, "Hand and Wrist Movement Control of Myoelectric Prosthesis Based on Synergy," *Human-Machine Systems, IEEE Transactions on,* vol. 45, pp. 74-83, 2015.

[10] E. N. Kamavuako, K. B. Englehart, W. Jensen, and D. Farina, "Simultaneous and proportional force estimation in multiple degrees of freedom from intramuscular EMG," *Ieee Transactions on Biomedical Engineering,* vol. 59, pp. 1804-1807, 2012.

[11] C. Lin, B. Wang, N. Jiang, and D. Farina, "Robust extraction of basis functions for simultaneous and proportional myoelectric control via sparse non-negative matrix factorization," *J Neuroeng Rehabil,* vol. 15, pp. 17-26, 2018/02/07 2018.

[12] P. Kim, K. S. Kim, and S. Kim, "Modified Nonnegative Matrix Factorization Using the Hadamard Product to Estimate Real-Time Continuous Finger-Motion Intentions," *IEEE Transactions on Human-Machine Systems,* vol. 47, pp. 1089-1099, 2017.

[13] D. D. Lee and H. S. Seung, "Learning the parts of objects by non-negative matrix factorization," *Nature,* vol. 401, pp. 788-798, 10/21/online 1999.

[14] A. Ebied, E. Kinney-Lang, L. Spyrou, and J. Escudero, "Evaluation of matrix factorisation approaches for muscle synergy extraction," MED ENG PHYS, vol. 57, pp. 51-60, 2018/07/01/ 2018.

[15] A. Cichocki, R. Zdunek, and S. Amari, "New Algorithms for Non-Negative Matrix Factorization in Applications to Blind Source Separation," in 2006 IEEE International Conference on Acoustics Speech and Signal Processing Proceedings, Toulouse, France, 2006.

[16] D. Yang, J. Li, X. Wang, and H. Liu, "Simultaneous estimation of 2-DOF wrist movements based on constrained non-negative matrix factorization and Hadamard product," Biomedical Signal Processing and Control, vol. 56, No. 101729, 2020